Dual-Band Complementary Split-Ring Resonator Engraved Rectangular Monopole for GSM and WLAN/WiMAX/5G Sub-6 GHz Band (New Radio Band)

Samuel Prasad Jones Christydass[1, *] and Nagarajan Gunavathi[2]

Abstract—In this paper, a rectangular monopole antenna engraved with a complementary split-ring resonator is proposed for dual-band operation. The proposed antenna is fabricated on an FR4 substrate with a dimension of $20 \times 34 \times 1.6\,\text{mm}^3$. The entire simulation is done using CST EM studio software. The proposed antenna exhibits dual-band operation from $1.78\,\text{GHz}$ to $1.90\,\text{GHz}$ and from $3.45\,\text{GHz}$ to $6.58\,\text{GHz}$. The band from $1.78\,\text{GHz}$ to $1.90\,\text{GHz}$ is due to the inclusion of CSRR, and its corresponding bandwidth is $120\,\text{MHz}$. It is validated with the quasi-static analysis. The permittivity characteristics of the proposed CSRR are retrieved using the NRW method and presented. The resonant frequency of the band created by the CSRR is $1.83\,\text{GHz}$ with $-37.68\,\text{dB}$ as its return loss values. The second wider band is due to the combination of the mode created by the CSRR along with the radiating patch from $3.45\,\text{GHz}$ to $6.58\,\text{GHz}$ with $3132\,\text{MHz}$ which has dual resonances at $3.65\,\text{GHz}$ and $5.59\,\text{GHz}$ with return losses of $-30.23\,\text{dB}$ and $-29.80\,\text{dB}$. The optimal values are chosen with the help of parametric analysis. The designed antenna is fabricated and measured. The measured results of return loss, gain, E-plane, and H-plane are compared with simulated ones, and they comply with each other. The dual-band operation, compact size, stable radiation pattern along with gain above $2.3\,\text{dBi}$ in the whole resonating band make it suitable for the GSM and WLAN/WiMAX/5G Sub-6 GHz band (new radio band).

1. INTRODUCTION

Many mobile devices provide services to various types of wireless applications like GPS, GSM, LTE, WLAN, and WiMAX in present-day modern communication systems. This present-day mobile device provides service for more than one application simultaneously, and at the same time, their primary requirement is compactness. The space available in these mobile devices for antenna placement is also minimal. The requirement mentioned above leads to the pursuit of a multiband antenna with compact size. This primary requirement of mobile devices attracts researchers to focus on the multiband antenna. The significant advantage of using a multiband antenna is that it reduces the number of antennas required for each application, and it also removes the filter used in the multiband system, which in turn reduces the complexity in fabrication, installation, and cost.

Numerous techniques have been used to achieve the multiband operation [1–3]. One of the broadest methods to realize the multiband response is the introduction of slots [4, 5] in the radiating element and ground plane [6, 7], and another method is the usage of different current paths produced by the inclusion of strips [8, 9]. In addition, other techniques such as Defected Ground Structures (DGS) [10], fractal [11], external active devices, and passive devices [12] have been used to realize the multiband functionalities. Even though the above techniques can realize the multiband operations, they impact

the design complexity, gain, and radiation pattern. The above-said disadvantage is overcome with the help of metamaterials (MTM) due to their unique electromagnetic properties, which are not available in nature. In the recent past, the disadvantages mentioned above are effectively overcome with the help of metamaterial structures.

Various metamaterial structures have been reported in the literature, and the properties such as refractive index, permittivity, and permeability will be negative at the designed frequency of operation. They are utilized in implementations of absorber, cloaking, filters, couplers, and antenna [13]. In a metamaterial-inspired antenna, the inclusion of metamaterial is capable of increasing the antenna parameters such as gain, directivity, and the number of operating bands. Compact size antenna with multiband using MTM is presented in [14]; the MTM is embedded in the substrate to reduce the radiating element size. The MTM substrates are used to achieve broader impedance matching and multiband [15]. In [16, 17], the directivity and gain are increased by the inclusion of the MTM in multiple operating frequencies. In [18], the metamaterial superstrates are employed, which increases gain. In all the above designs, the overall size is increased due to the addition of MTM as a separate layer. In the last decade, usage of the MTM in the radiating element and ground has been increased to improve the antenna performance. The Split Ring Resonator (SRR) and Complementary Split Ring Resonator (CSRR) are the two broadly used MTM structures for overcoming the disadvantage of increased size. The MTM CSRR arrays of various shapes [19, 20] are used to increase bandwidth [21] and impedance matching [22]. In [23], multiple CSRR rings are utilized to realize the directional antenna; as the number of CSRR rings increases, the resonant frequency of the structure decreases. MTM structures like single ring CSRR [24, 25], SRR [26, 27], Open Complementary Split Ring Resonators (OCSRR) [28], Electric-Inductive-Capacitive (ELC) resonator [29] are engraved in the patch for the size reduction, gain, and bandwidth increment. But a minimal amount of work has been focused on the MTM for realizing multiband functionalities.

In this paper, a CSRR loaded rectangular monopole is proposed for dual-band operation. The operating band in the range 1.78 GHz to 1.90 GHz covers GSM, and the range 3.45 GHz to 6.58 GHz covers WiMAX, WLAN, and 5G sub 6 GHz new radio band (n77, n78, and n79 bands). The reduced ground structure is exploited to expand the impedance bandwidth. The CSRR designed at 1.8 GHz is engraved in the radiating element to cover the 1.83 GHz band. The result of including the CSRR is validated with the aid of permittivity extraction NicolsonRossWeir (NRW) method and quasi-static analysis. The critical parameters are identified with parametric analysis. The simulated antenna parameters are on par with the measured results. The proposed structure can operate at multiple bands covering the most needed wireless applications, including GSM, WLAN, WiMax, and sub 6 GHz band new radio application. The overall size of $20 \times 34 \, \text{mm}^2$ results in a compact design, making the integration easy. Compact structure, good gain, stable radiation pattern, and broader bandwidth are significant features of the proposed antenna. The above-said feature of the proposed antenna makes it more suitable for the current 5G based multi-application wireless devices. The integration of the traditional wireless standards along with the new radio 5G standards is the additional advantage of the proposed system. In Section 2, the evolution stage is presented, followed by the CSRR analysis in Section 3. In Section 4, the results are discussed, and the observations are concluded in Section 5.

2. DESIGN OF CSRR LOADED RECTANGULAR MONOPOLE

The proposed CSRR engraved dual-band rectangular monopole patch antenna is designed using CST EM software. The structure is designed and fabricated on an FR4 substrate with a loss tangent value of 0.002 dielectric constant of 4.4, and thickness (h) of 1.6 mm. The proposed structure has 4 design configurations, and it is depicted in Fig. 1. A simple rectangular monopole antenna is designed to operate at 3.5 GHz, which is configuration 1. Then in order to expand the impedance bandwidth, the reduced ground technique is used in configuration 2. Then in configuration 3, a closed ring slot is engraved in the radiating element, which affects the impedance due to the change in the current direction. In the final configuration, a CSRR, which is designed at 1.8 GHz, is engraved. In Fig. 2, the proposed antenna geometry and its parameters are presented. In Table 1, the parameter values are listed. The dimension of the designed structure is $20 \times 34 \times 1.6 \, \text{mm}^3$. The proposed antenna exhibits dual-band operation — 1.78 GHz to 1.90 GHz with 1.83 GHz as its resonance and 3.45 GHz to 6.58 GHz
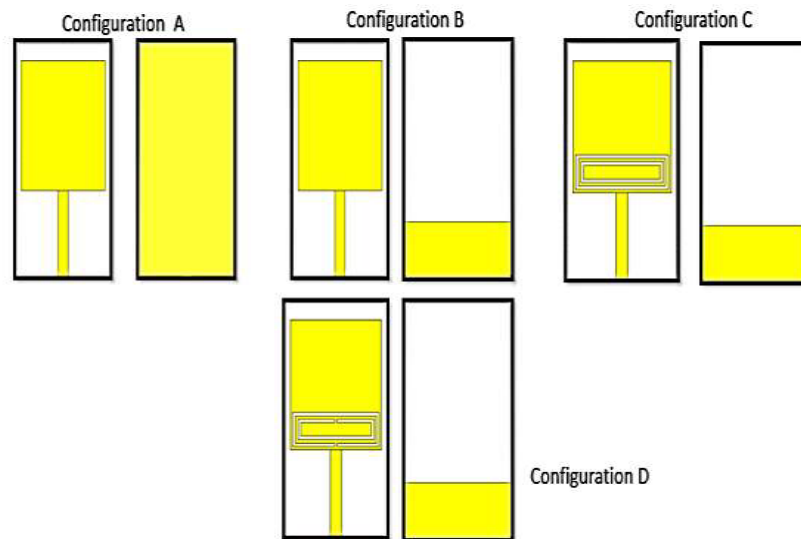
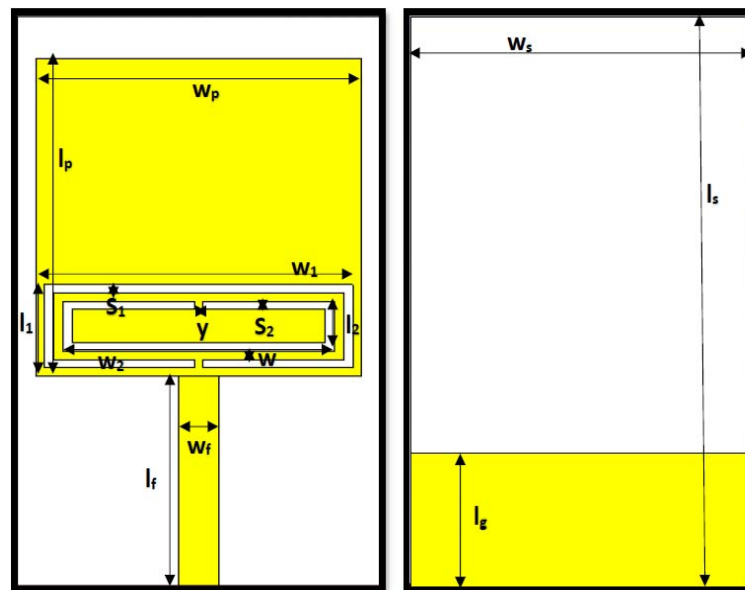**Figure 1.** Evolution of CSRR engraved rectangular antenna.

Figure 2. Geometry of CSRR engraved rectangular antenna and its parameters.

with dual resonances at 3.65 GHz and 5.59 GHz, respectively. Configuration 2 with a reduced ground structure is capable of achieving the wider impedance bandwidth. In configuration 3, the bandwidth is reduced due to the capacitive effect of the closed rings. In configuration 4, a CSRR is engraved to form triband. The two rings change the current path, based on their dimensions, and the two resonances at 3.65 GHz and 1.83 GHz are achieved along with the patch resonance of 5.59 GHz.

The seed antenna configuration 1 is designed on a double-sided FR4 substrate with a rectangular radiating element of size $w_p \times l_p$ on top of the substrate, and the ground plane of size $w_s \times l_s$ is printed on the other side. The antenna is designed using the equation below.

$$W = \frac{c}{2f_r}\sqrt{\frac{2}{\varepsilon_r + 1}} \tag{1}$$

**Table 1.** CSRR engraved rectangular antenna parameters (in mm).

w_s	l_s	l_g	w_p	l_p	w_f	l_f	h
20	34	8	18	19	2.2	12.5	1.6
w_1	l_1	w_2	l_2	s_1	s_2	w	y
16.5	4.5	14.5	2.5	0.5	0.5	0.5	0.25

$$L = \frac{c}{2f_r\sqrt{\varepsilon_{\text{eff}}}} - 2\Delta L \tag{2}$$

$$\varepsilon_{\text{eff}} = \frac{\varepsilon_r + 1}{2} + \frac{\varepsilon_r - 1}{2}\left[1 + \frac{12h}{W}\right]^{\frac{-1}{2}} \tag{3}$$

$$\Delta L = 0.412h\frac{(\varepsilon_{\text{eff}} + 0.3)}{(\varepsilon_{\text{eff}} - 0.258)}\frac{\left(\dfrac{W}{h} + 0.264\right)}{\left(\dfrac{W}{h} + 0.8\right)} \tag{4}$$

where c, f_r, h, and ε_{eff} are the speed of light, resonant frequency, substrate height, and effective dielectric constant, respectively. In configuration 2, in order to expand the impedance bandwidth, the ground length of 34 mm in configuration 1 is reduced to 8 mm. As a result, it has wide bandwidth from 3.43 GHz to 6.59 GHz with a bandwidth of 3132 MHz. Next, a closed ring slot is introduced in the radiating element; due to the change in the current path and the introduction of capacitance, the impedance bandwidth is reduced. Configuration 3 has dual-band operations from 4.94 GHz to 5.42 GHz and from 6.01 GHz to 6.37 GHz. Finally, in configuration 4, the proposed antenna is designed by engraving the CSRR designed at 1.8 GHz in the rectangular radiating element at the maximum surface current region. The CSRR creates a new resonance at 1.83 GHz based on its geometrical values. Hence, the proposed antenna operates at dual bands with centre frequencies 1.83 GHz and 4.95 GHz. In Fig. 3, the return loss characteristics of the proposed antenna and its evolution stages are presented.
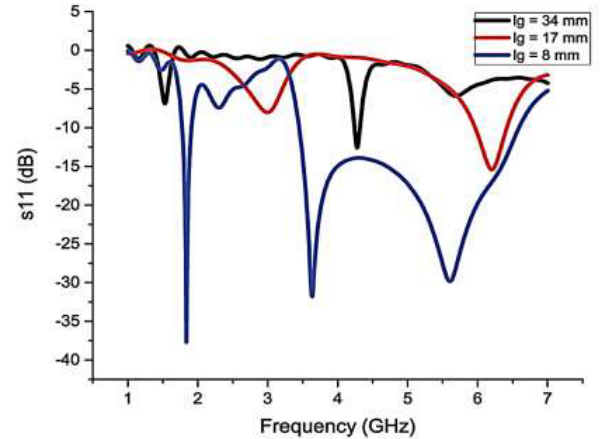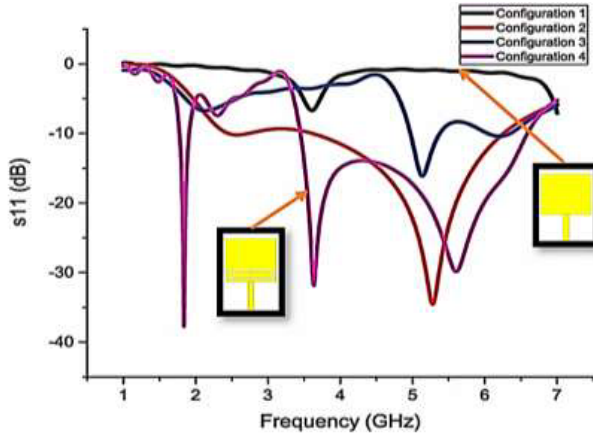
Figure 3. S_{11} comparison (Configuration 1 to 4).   **Figure 4.** Ground length analysis.

The ground length is reduced to achieve good impedance bandwidth. Its corresponding analysis is presented in Fig. 4; from the figure, we can observe that $l_g = 8$ mm is the optimum dimension for excellent impedance bandwidth. Hence, these two values are chosen for the final fabrication.

3. RECTANGULAR CSRR EQUIVALENT CIRCUIT AND QUASI-STATIC ANALYSIS

3.1. Effect of CSRR Rings

The proposed antenna has a dual-band operation with a centre frequency at 1.83 GHz and 4.85 GHz. The second band has dual resonances at 3.65 GHz and 5.59 GHz. The CSRR rings and slit in the rings are responsible for the multiband operation. The effect of CSRR rings is confirmed with the help of the return loss comparison graph projected in Fig. 5. Two cases are presented in the figure — case 1 is a single ring, and case 2 is double rings. The single ring is capable of having wider impedance matching due to the combination of patch mode and the mode generated by the CSRR. The single ring antenna has an active region from 3.20 GHz to 6.38 GHz with dual resonances at 3.33 GHz and 5.44 GHz. In case 2 double rings create a new band at 1.83 GHz, and it shifts the frequency band created by a single ring without affecting the bandwidth. The final proposed antenna is achieved by the bandwidth of 120 MHz at 1.83 GHz and 3132 MHz at centre frequency 4.95 GHz.
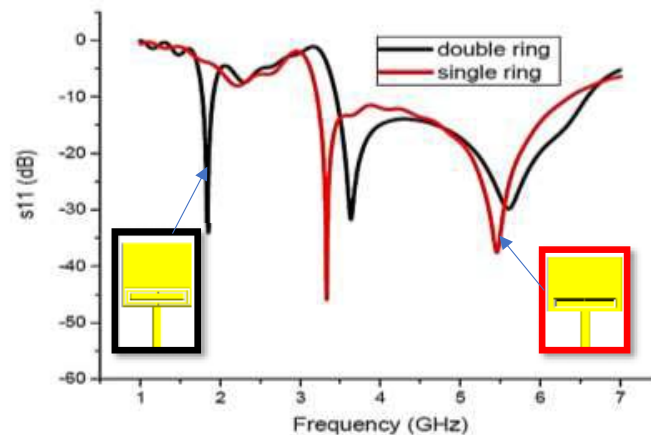

Figure 5. Effect of CSRR rings.

3.2. Parametric Analysis

The CSRR is engraved in the radiating element, which in turn creates a 1.83 GHz resonating band. This band totally depends on the CSRR geometric parameters. Therefore, these geometrical parameters are critical in the proposed design, and its optimum dimension is chosen with the help of parametric analysis.

The width (s_1) of CSRR outer ring slot is increased in steps of 0.25 mm from 0.25 mm to 0.75 mm. The simulated s_{11} for various values of s_1 is depicted in Fig. 6; from the figure, we can clearly observe that $s_1 = 0.5$ mm achieves suitable impedance matching in all the resonating bands. A shift in the 1.83 GHz band is observed, from which we can infer that the outer CSRR ring is responsible for the 1.83 GHz band. Then similarly, the inner ring slot width (s_2) is increased from 0.25 mm to 0.75 mm in steps of 0.25 mm. The comparison of the return loss performance for various values of s_2 is presented in Fig. 7. From the figure, we can observe that $s_2 = 0.5$ mm produces good impedance matching and maintains impedance bandwidth in all the resonating bands. There is a shift in the resonant frequency at 3.65 GHz as the value of s_2 is changed; from that, we can observe that the inner ring is responsible for the 3.65 GHz band.

In Fig. 8, the s_{11} for various values of slit width (y) is presented. It can be observed that $y = 0.25$ mm has good impedance matching in all the resonating bands from the figure. So, it is chosen as the final value for fabrication.
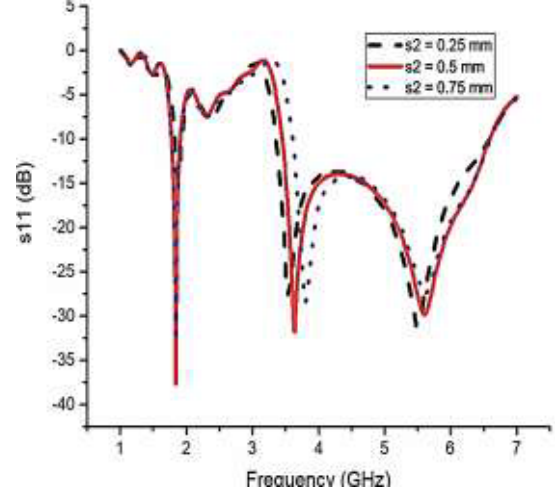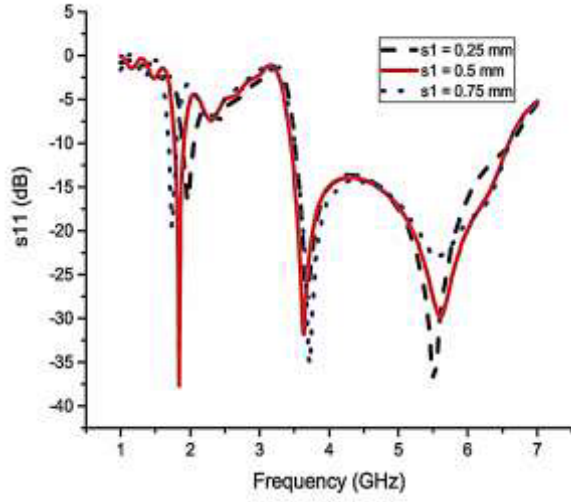
Figure 6. s_{11} evaluation for various values of s_1.   **Figure 7.** s_{11} evaluation for various values of s_2.
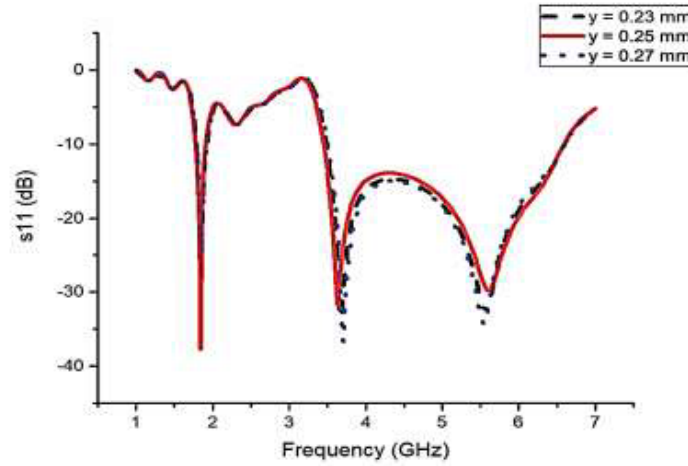

Figure 8. s_{11} evaluation for various values of y.

3.3. Quasi-Static Analysis

In Fig. 9, the proposed CSRR equivalent circuit structure is depicted. The resonant frequency of the CSRR is calculated from Equation (7). The inductance L_{CSRR} and capacitance C_{CSRR} of the CSRR is calculated [29] using Equation (5) and Equation (6), respectively.

$$
\begin{aligned}
L_{\text{CSRR}} \;=\; & 4 * \mu_0 * [l - (N-1)(w+s)] * \left[\ln\left(\frac{0.98 * [l - (N-1)(w+s)]}{(N-1)(w+s)} \right) \right. \\
& \left. + \left(\frac{1.84 * [l - (N-1)(w+s)]}{(N-1)(w+s)} \right) \right]
\end{aligned}
\tag{5}
$$

$$
C_{\text{CSRR}} \;=\; \frac{N-1}{2} * [2l - (2N-1)(w+s)] * \varepsilon_0 * \left(\frac{K(\sqrt{1-k^2})}{K(k)} \right)
\tag{6}
$$
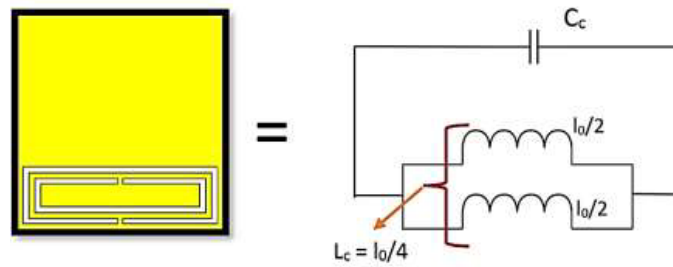
Figure 9. Equivalent circuit of CSRR.

where $k = \frac{s}{2w+s}$

$$F = \frac{1}{2\Pi\sqrt{L_{\mathrm{CSRR}} * C_{\mathrm{CSRR}}}} \tag{7}$$

where N is the number of rings, w the slot width, l the average length, S the spacing between the slots, and K a complete elliptic integral of the first kind. Equations (5) to (7) are implemented in MATLAB to calculate the inductance, capacitance, and resonant frequency of the CSRR. The above equation is true for $N > 1$. For $N = 2$, the average length is equal to 8.5 mm, $L_{\mathrm{CSRR}} = 8.447 \times 10^{-8}$ H and $C_{\mathrm{CSRR}} = 8.889 \times 10^{-14}$ F. From Equation (7), the resonant frequency of CSRR is equal to 1.83×10^9 Hz. This analysis authenticates that the CSRR engraved in the radiating element is responsible for the 1.83 GHz band.

### 3.4. Rectangular CSRR Permittivity Extraction

The negative permittivity, which is observed from Fig. 11, is based on the dimension of the CSRR structure. The CSRR can create a new resonance at 1.83 GHz, which can be verified with the help of the permittivity extraction NRW method. The negative permeability of the proposed CSRR is also presented in Fig. 12. The proposed structure has a negative permeability at 2.25 GHz. The designed CSRR is placed in a waveguide setup as shown in Fig. 10. An appropriate boundary condition is specified for the extraction of the transmission and reflection coefficient. Through the input port, the EM wave is used to excite the CSRR, and at the output port, the s parameter coefficients are retrieved.
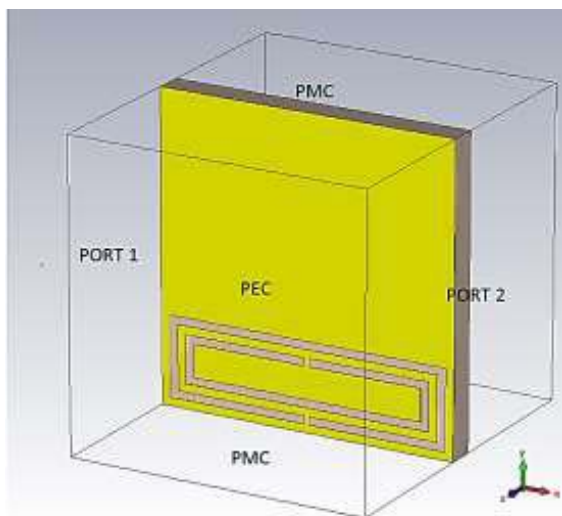
Figure 10. S parameter extraction set up.
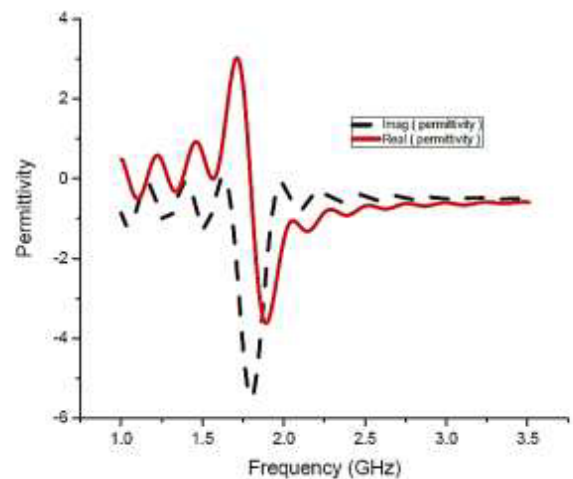
Figure 11. Negative permittivity of the proposed CSR.
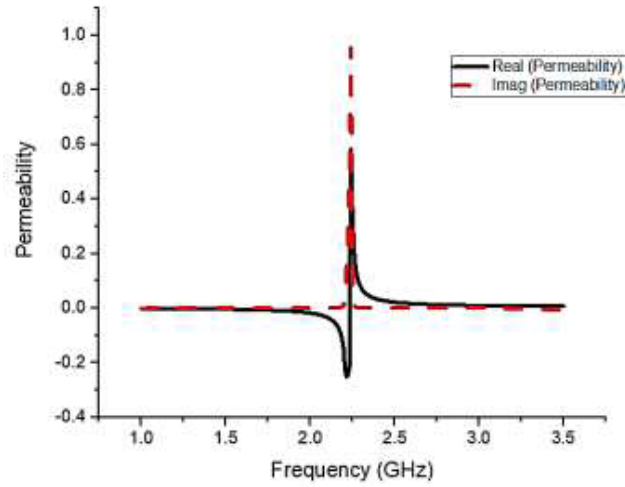
Figure 12. Negative permeability of the proposed CSRR.

With retrieved s_{11} and s_{21}, using the NRW method [30, 31], the permittivity and permeability of the proposed CSRR are extracted.

$$\mu_r = \frac{2}{jK_O d} * \frac{1 - V_2}{1 + V_2} \tag{8}$$

$$\varepsilon_r = \frac{2}{jK_O d} * \frac{1 - V_1}{1 + V_1} \tag{9}$$

where d is the thickness of the substrate, K_0 the free space wave number, $V_1 = S_{21} - S_{11}$ and $V_2 = S_{21} + S_{11}$.

3.5. Equivalent Circuit

In Fig. 13, the proposed CSRR engraved rectangular antenna equivalent circuit is presented. Z_0 is the characteristic impedance, and l_f and R_f are the electrical lengths of the transmission line and loss resistance, respectively. The rectangular antenna is represented using the parameters R_{ra}, C_{ra}, and L_{ra}. C_{CSRR} due to the capacitance across the slot and L_{CSRR} due to the metal region represent the
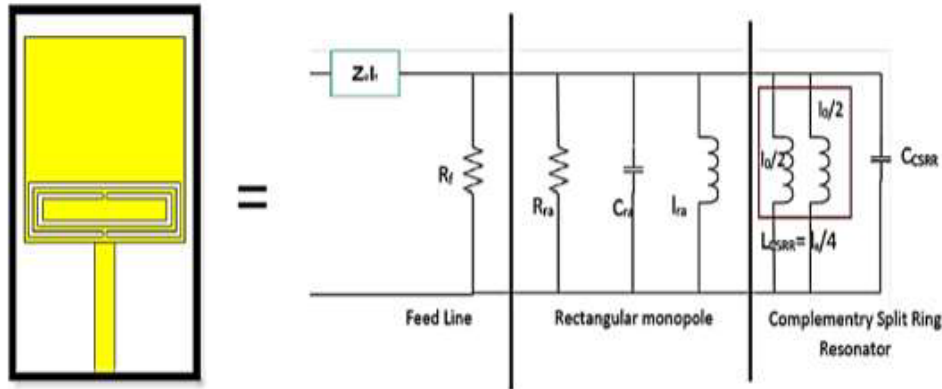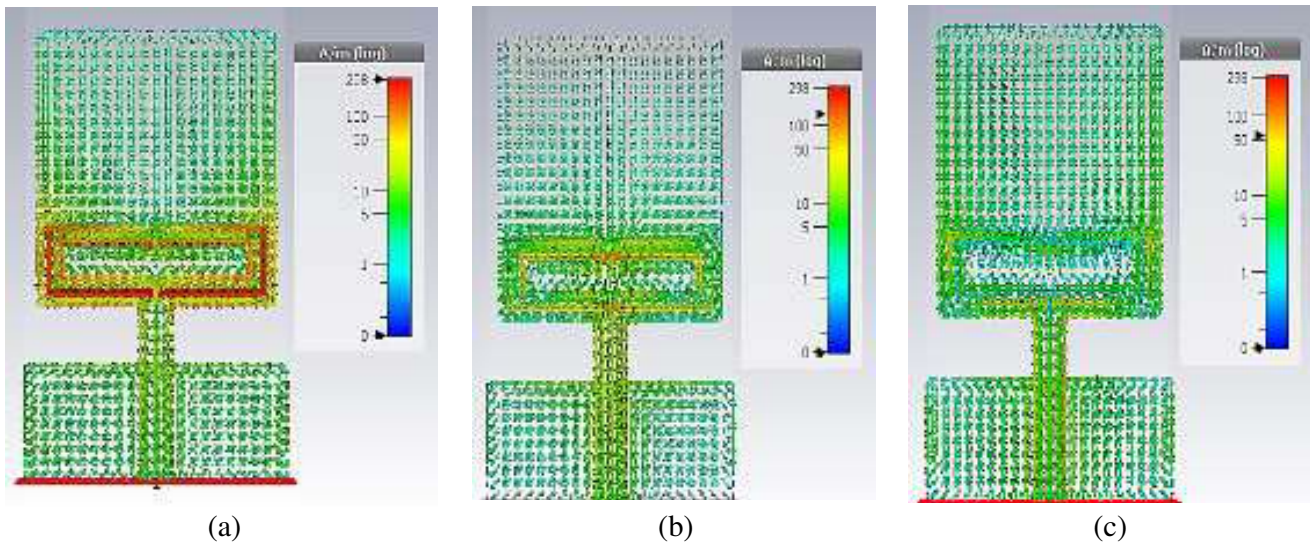

Figure 13. Equivalent circuit of the proposed antenna.

CSRR. The resonant frequency of the CSRR is given by

$$f_0 = \frac{1}{2\Pi\sqrt{C_{\text{CSRR}}L_{\text{CSRR}}}} \tag{10}$$

4. RESULT AND DISCUSSION

The surface current distribution of the CSRR engraved rectangular antenna at various resonating bands is presented in Fig. 14. The figure shows that the maximum surface current is centred around the outermost CSRR ring at 1.8 GHz, and hence it is responsible for this band. The negative permittivity

(a) (b) (c)

Figure 14. Surface current distribution at the various resonating frequency. (a) 1.83 GHz, (b) 3.65 GHz, (c) 5.59 GHz.

Table 2. Proposed antenna vs other references.

Reference Number	Technique used	Dimensions (mm)	Resonant Frequency (GHz)	Equivalent Circuit Analysis	Metamaterial Property Verification
4	Slotted patch	25 × 25	2.41 to 6.10 and 9.40 to 13.81	Not Presented	Not Applicable
7	U shaped patch with slot	30 × 30	3.31 to 3.60 and 5.10 to 6.00	Not Presented	Not Applicable
13	Slot	21 × 28	5.00 to 6.12 and 7.70 to 8.51	Not Presented	Not Applicable
21	Elliptical-ring with split-triangular patch	30 × 33	2.52 to 2.62 and 3.31 to 3.64	Not Presented	Not Applicable
22	patches in ground	60 × 180	0.66 to 0.79 and 3.28 to 3.78	Not Presented	Not Applicable
25	CSRR and reduced ground	20 × 25	3.90 to 4.96 and 6.70 to 11.2	Not Presented	Not Presented
27	SRR	22 × 24	2.40 to 2.74 and 3.25 to 3.64	Not Presented	Not Presented
Proposed	CSRR	20 × 34	1.78 to 1.90 and 3.45 to 6.58	Presented	Presented

is observed at 1.8 GHz in Fig. 11; we can conclude that the CSRR engraved in the radiating element is responsible for 1.83 GHz. The 1.83 GHz is also validated with the quasi-static analysis presented in Section 3.3. At 3.65 GHz band, the surface current is distributed in the innermost ring, and at 5.59 GHz, the current is distributed over the entire antenna. The CSRR frequency 3.65 GHz and patch frequency 5.59 GHz are combined to achieve wider impedance bandwidth of 3132 MHz. In Table 2, the proposed antenna is compared with the already available antenna in the literature.

A Mask is prepared initially for the fabrication, which contains the negative of the proposed design. A double side copper-clad FR4 substrate is cleaned with acetone; after it is dried up, the structure is laminated with a negative photoresist film. The mask prepared is attached to the laminated copper-clad FR4 substrate and exposed to UV light. Then, it is dissolved in the developer solution made up of sodium carbonate followed by etching using Ferric Chloride solution. The hardened photoresist is removed with sodium hydroxide. With the photolithography chemical etching method, the proposed antenna is fabricated.

In Fig. 15, both simulated E-plane and H-plane radiation patterns are compared with the measured results. The anechoic chamber setup is also presented in Fig. 15(d). In all the resonating bands, the proposed structure exhibits a stable radiation pattern. It is professed from the figure that the CSRR

(a)   (b)

(c)   (d)
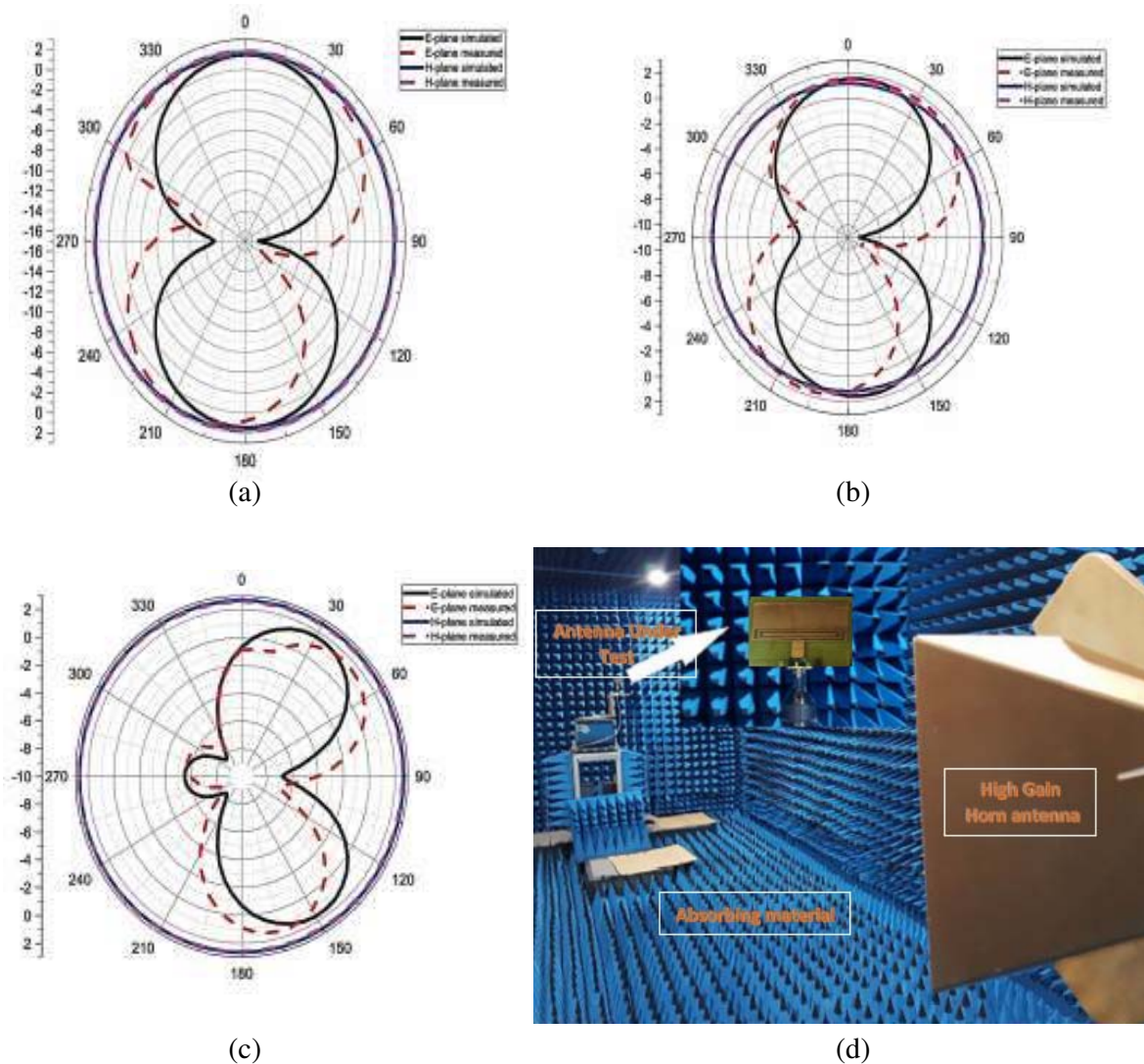
Figure 15. E plane and H plane (measured vs simulated) at the various resonating frequency and measurement setup. (a) 1.83 GHz, (b) 3.65 GHz, (c) 5.59 GHz, (d) chamber set up.
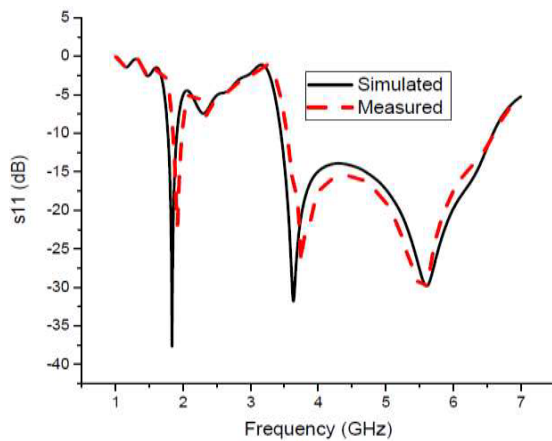
Figure 16. Fabricated prototype.

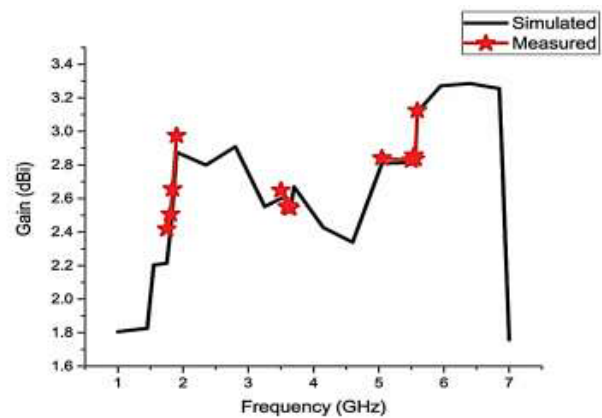**Figure 17.** Simulated vs. measured s_{11}.

Figure 18. Measured and simulated gain comparison.

engraved rectangular monopole antenna has an omnidirectional H-plane pattern and eight-shaped dipole E-plane pattern. In Fig. 16, the fabricated prototype is presented, and it is measured using VNA Anritsu S820E. The measured result is compared with the simulated ones and presented in Fig. 17. The deviation between the results is due to the connector error at high frequency and fabrication inadequacy.

The measured and simulated gains of the proposed prototype antenna are presented in Fig. 18. The proposed and simulated gains are on par with each other, with the gain maintained above 2.3 dBi in all the resonating bands. The maximum gain of 3.16 dBi is observed from the figure below. In Table 3, the simulated results are tabulated against the measured results.

Table 3. Simulated vs. measured.

Simulated				Measured			
Resonant Frequency (GHz)	Operating band (GHz)	Return loss (dB)	Impedance Bandwidth (MHz)	Resonant Frequency (GHz)	Operating band (GHz)	Return loss (dB)	Impedance Bandwidth (MHz)
1.83	1.78 to 1.90	−37.68	120	1.91	1.84 to 1.98	−21.97	140
3.637	3.45 to 6.58	−31.81	3132	3.754	3.75 to 5.50	−26.82	3060
5.59		−29.79		5.509		−30.22	

5. CONCLUSION

A metamaterial-inspired rectangular antenna is presented for GSM and WLAN/WiMAX/5G Sub-6 GHz band (new radio band). The proposed antenna exhibits dual-band operation from 1.78 GHz to 1.90 GHz and from 3.45 GHz to 6.58 GHz. The 1.83 GHz band is introduced due to the inscription of a CSRR on the radiating element, which is validated with the quasi-static analysis and permittivity extraction. Another band with wider bandwidth of 3132 MHz is due to the combination of CSRR and rectangular patch modes, which is validated with the help of simulated surface current results. The optimum values of the critical parameters like CSRR dimensions, feed width, and ground length are chosen with the help of parametric analysis, and it is also presented in the article. The depicted simulated results of S_{11}, gain, E plane, and H-plane pattern comply with the measured ones. Simple design, compact size, good gain, impedance matching, and stable radiation pattern are the significant features of the proposed antenna.

REFERENCES

1. Liu, P., Y. Zou, B. Xie, X. Liu, and B. Sun, "Compact CPW-fed tri-band printed antenna with meandering split-ring slot for WLAN/WiMAX applications," *IEEE Antennas Wireless Propag. Lett.*, Vol. 11, 1242–1244, 2012.
2. Li, D. and J.-F. Mao, "Multiband multimode arched bow-shaped fractal helix antenna," *Progress In Electromagnetics Research*, Vol. 141, 47–78, 2013.
3. Xu, P., Z.-H. Yan, and C. Wang, "Multiband modified fork-shaped monopole antenna with dual L-shaped parasitic plane," *Electron. Lett.*, Vol. 47, No. 6, 364–365, 2011.
4. Baudha, S. and D. K. Vishwakarma, "Miniaturized dual broadband printed slot antenna with parasitic slot and patch," *Microw. Opt. Technol. Lett.*, Vol. 56, No. 10, 2260–2265, 2014.
5. Chaurasia, P., B. K. Kanaujia, S. Dwari, and M. K. Khandelwal, "Design and analysis of seven-bands-slot-antenna with small frequency ratio for different wireless applications," *AEU — International Journal of Electronics and Communications*, Vol. 99, 100–109, 2019.
6. Al-Tumah, W. A. G., R. M. Shaaban, and A. Tahir, "Design, simulation and measurement of triple band annular ring microstrip antenna based on shape of crescent moon," *AEU — International Journal of Electronics and Communications*, Vol. 117, 2020.
7. Shan, K., C. L. Ruan, and L. Peng, "Design of a novel planar ultrawideband antenna with 3.5 and 5.5 GHz dual band notched characteristics," *Microw. Opt. Technol. Lett.*, Vol. 53, 370–375, 2011.
8. Iqbal, A., A. Bouazizi, O. A. Saraereh, A. Basir, and R. K. Gangwar, "Design of multiple band, meandered strips connected patch antenna," *Progress In Electromagnetics Research Letters*, Vol. 79, 51–57, 2018.
9. Basar, M. R., M. A. Hossain, M. R. U. Hoque, and K. M. Morshed, "Compact dual l-slit slotted antenna for spacecraft, WLAN, Wi-Fi, and bluetooth application," *2012 7th International Conference on Electrical & Computer Engineering (ICECE)*, 706–708, IEEE, 2012.
10. Liu, G., M. Fang, R. Zhi, J. Bai, and Z. Zeng, "Compact CPW-fed multiband antenna for TD-LTE/WLAN/WiMAX applications," *Progress In Electromagnetics Research Letters*, Vol. 65, 9–14, 2017.
11. Ran, X., Z. Yu, T. Xie, Y. Li, X. Wang, and P. Huang, "A novel dual-band binary branch fractal bionic antenna for mobile terminals," *International Journal of Antennas and Propagation*, Vol. 2020, Article ID 6109093, 9 pages, 2020, https://doi.org/10.1155/2020/6109093.
12. Promwong, S. and A. Pinsakul, "A monolithic patch antenna on a semi-insulated Alumina ($Al_2O_3Al_2O_3$) substrate for active integrated antenna," *Wireless Personal Communications*, Vol. 115, 2755–2765, 2020.
13. Liu, C. Y., T. Jiang, and Y. S. Li, "A compact wide slot antenna with dual band-notch characteristic for ultra-wideband applications," *Journal of Microwaves, Optoelectronics and Electromagnetic Applications*, Vol. 10, No. 1, 55–64, 2011.

14. Ouedraogo, R. O., E. J. Rothwell, A. R. Diaz, K. Fuchi, and A. Temme, "Miniaturization of patch antennas using a metamaterial-inspired technique," *IEEE Trans. Antennas Propag.*, Vol. 60, 2175–2182, 2012.

15. Weng, Z. B., Y. C. Jiao, F. S. Zhang, Y. Song, and G. Zhao, "A multiband patch antenna on metamaterial substrate," *Journal of Electromagnetic Waves and Applications*, Vol. 22, 445–452, 2008.

16. Arora, C., S. S. Pattnaik, and R. N. Baral, "SRR superstrate for gain and bandwidth enhancement of microstrip patch antenna array," *Progress In Electromagnetics Research B*, Vol. 76, 73–85, 2017.

17. Al-Bawri, S. S., S. Islam, H. Y. Wong, and M. F. Jamlos, "Bandwidth and gain enhancement of quad-band CPW-fed antenna for wireless applications," *Sensors*, Vol. 20, No. 2, 1–14, 2020.

18. Patel, S. K., C. Argyropoulos, and Y. P. Kosta, "Broadband compact microstrip patch antenna design loaded by multiple split ring resonator superstrate and substrate," *Waves in Random and Complex Media*, Vol. 5030, 1–12, 2016.

19. Liu, T., X. Y. Cao, J. Gao, Q. Yang, and W. Q. Li, "Design of miniaturized broadband and high gain metamaterial patch antenna," *Microw. Opt. Technol. Lett.*, Vol. 53, 2858–2861, 2011.

20. Zhao, X., Y. Lee, and J. Choi, "Design of a compact patch antenna using split-ring resonator embedded substrate," *Microw. Opt. Technol. Lett.*, Vol. 53, 2786–2790, 2011.

21. Dattatreya, G. and K. K. Naik, "A low volume flexible CPW-fed elliptical-ring with split-triangular patch dual-band antenna," *Int. J. RF Microw. Comput. Aided Eng.*, Vol. 29, 2019.

22. Arya, A. K., S. J. Kim, and S. Kim, "A dual-band antenna for LTE-R and 5G lower frequency operations," *Progress In Electromagnetics Research Letters*, Vol. 88, 113–119, 2020.

23. Naoui, S., L. Latrach, and A. Gharsallah, "Metamaterials microstrip patch antenna for wireless communication RFID technology," *Microw. Opt. Technol. Lett.*, Vol. 57, 1060–1066, 2015.

24. Pandeeswari, R., "SRR and NBCSRR inspired CPW fed triple band antenna with modified ground plane," *Progress In Electromagnetics Research C*, Vol. 80, 111–118, 2018.

25. Naik, K. K., "Asymmetric CPW-fed SRR patch antenna for WLAN/WiMAX applications," *AEU — International Journal of Electronics and Communications*, Vol. 93, 103–108, 2018.

26. Geetharamani, G. and T. Aathmanesan, "Design of metamaterial antenna for 2.4 GHz WiFi applications," *Wireless Personal Communications*, Vol. 113, No. 4, 2289–2300, 2020.

27. Boopathi Rani, R. and S. Pandey, "A CPW-fed circular patch antenna inspired by reduced ground plane and CSRR slot for UWB applications with notch band," *Microw. Opt. Technol. Lett.*, Vol. 59, 745–749, 2017.

28. Herraiz-Martínez, F. J., G. Zamora, F. Paredes, F. Martín, and J. Bonache, "Ultiband printed monopole antennas loaded with OCSRRs for PANs and WLANs," *IEEE Antennas and Wireless Propagation Letters*, Vol. 10, 1528–1531, 2011.

29. Sam, P. J. C. and N. Gunavathi, "A tri-band monopole antenna loaded with circular electric-inductive-capacitive metamaterial resonator for wireless application," *Applied Physics A: Materials Science and Processing*, Vol. 126, No. 10, 1–11, 2020.

30. Daniel, R. S. and R. Selvaraj, "A low-profile spilt ring monopole antenna loaded with hexagonal split ring resonator for RFID applications," *Progress In Electromagnetics Research M*, Vol. 92, 169–179, 2020.

31. Prasad Jones Christydass, S. and N. Gunavathi, "Octa-band metamaterial inspired multiband monopole antenna for wireless application," *Progress In Electromagnetics Research C*, Vol. 113, 97–110, 2021.